American Mineralogist, Volume 72, pages 382–391, 1987

Electron-diffraction and electron-microscopy study of balangeroite and gageite: Crystal structures, polytypism, and fiber texture

Giovanni Ferraris
Dipartimento di Scienze della Terra, Università di Torino, Via S. Massimo 22, 10123 Torino, Italy
Marcello Mellini
C.N.R., Centro di Geologia Strutturale e Dinamica dell'Appennino, Via S. Maria 53, 56100 Pisa, Italy
Stefano Merlino
Dipartimento di Scienze della Terra, Università di Pisa, Via S. Maria 53, 56100 Pisa, Italy

Abstract

Electron-diffraction and transmission-electron microscopy (TEM) investigations were carried out on the fibrous minerals balangeroite and gageite. The studies indicated for balangeroite a monoclinic unit cell with $a_m = 19.40$, $b_m = 19.40$, c_m (unique axis) = 9.65 Å, $\gamma_m = 88.9°$; two polytypic modifications were found for gageite: gageite 2M, monoclinic, isostructural with balangeroite, cell dimensions $a_m = 19.42$, $b_m = 19.42$, $c_m = 9.84$ Å, $\gamma_m = 89.5°$, and gageite 1Tc, triclinic, unit-cell dimensions $a_t = 14.17$, $b_t = 14.07$, $c_t = 9.84$ Å, $\alpha_t = 76.5°$, $\beta_t = 76.6°$, $\gamma_t = 86.9°$.

Chemical and physical data pointed to the presence of four-repeat silicate chains (T), running in the channels of the octahedral framework described by Moore (1969) and placed on both sides of Moore's octahedral walls (O) to give rise to composite TOT modules, interconnected through octahedral bundles. The corresponding ideal crystal-chemical formula is $M_{42}O_6(OH)_{40}(Si_4O_{12})_4$, with M denoting cations in octahedral coordination, mainly Mg in balangeroite and Mn in gageite.

The monoclinic and triclinic structural arrangements may be described as consisting of equivalent layers, characterized by translation periods a_m and c_m and width $b_o = b_m/2$. Adjacent layers are related by the vector $\mathbf{t}_1 = -\mathbf{a}_m/2 + \mathbf{b}_o + \mathbf{c}_m/3$ or the vector $\mathbf{t}_2 = -\mathbf{a}_m/2 + \mathbf{b}_o - \mathbf{c}_m/3$. The layer sequence $\mathbf{t}_1\mathbf{t}_2\mathbf{t}_1\mathbf{t}_2 \ldots$ is realized in the monoclinic modifications, whereas the sequence $\mathbf{t}_1\mathbf{t}_1\mathbf{t}_1 \ldots$ (or $\mathbf{t}_2\mathbf{t}_2\mathbf{t}_2 \ldots$) is realized in the triclinic modification. The symmetry properties of the two arrangements, the peculiar features of their diffraction patterns, and the appearance of diffuse spots in various patterns are discussed and explained on the basis of the OD (order-disorder) theory.

Finally, TEM evidence for the replacement of balangeroite by chrysotile during retrograde metamorphism is given, and the role of that mineral in the metamorphism of ultramafic rocks is discussed.

Introduction

Gageite is a fibrous manganese silicate that was found in low-temperature hydrothermal veins at Franklin, New Jersey. Although the complete structure determination was hampered by the disordered nature of the mineral, Moore (1969) was able to outline a substructure, with reference to an orthorhombic cell with $a = 13.79$, $b = 13.68$, $c' = 3.279$ Å, space group *Pnnm* ($a \times b \times c'$ cell hereafter), disregarding the indications for a trebled c parameter that were suggested by the occurrence of additional diffuse and weak reflections.

The substructure consists of two kinds of interlinked modules, both of which are built up by chains of edge-sharing octahedra: walls three chains wide (3×1 walls) and bundles that extend two chains both in width and thickness (2×2 bundles). Each module shares its free corners with the doubly shared corners of the other module. The resulting octahedral framework contains [001] pipelike channels that, according to Moore (1969), house disordered silicate tetrahedra.

Although the topology of the octahedral framework seemed to be quite well defined, the proposed number and the disordered arrangement of the tetrahedra in the channels were probably an artifact of the assumed substructure. In fact, as regards their number, Dunn (1979) derived, on the basis of new chemical analyses, $(Mn,Mg,Zn)_{40}Si_{15}O_{50}(OH)_{40}$ as the chemical content of a cell with trebled c parameter; this empirical formula does not agree with the crystal-chemical formula $(Mn,Mg,Zn)_{42}(Si_{12}O_{36})[O_6(OH)_{48}]$ proposed by Moore (1969).

0003–004X/87/0304–0382$02.00

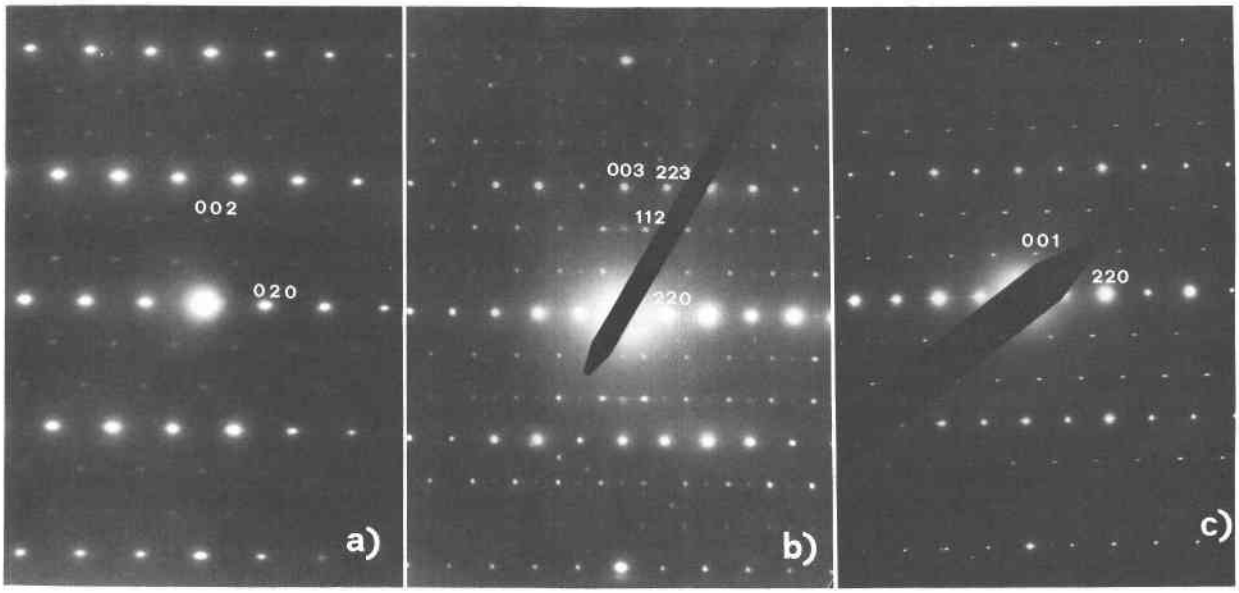

Fig. 1. Electron-diffraction patterns (c* vertical). (a) Balangeroite [100]; the reflections are indexed with reference to the $2a \times 2b \times c$ cell. The strongest spots, $l = 3n$, correspond to the $a \times b \times c'$ cell. (b) Balangeroite [1$\bar{1}$0]; the reflections are indexed with reference to the $2a \times 2b \times c$ cell. The 003 spot, kinematically forbidden, arises by dynamical effects (Gjonnes and Moodie, 1965) and vanishes with a change in orientation (e.g., Fig. 1a). The four different classes of reflections (absent, weak, medium, strong) may be clearly observed in this diffraction pattern. (c) Gageite 1Tc [1$\bar{1}$0]; the reflections are indexed with reference to the primitive triclinic cell.

More recently, Compagnoni et al. (1983) described a new fibrous silicate, balangeroite, the Mg-dominant analogue of gageite. From [001] rotation photographs, which clearly indicated a trebled c parameter, and by least-squares fitting of the X-ray powder-diffraction pattern, the parameters $a = 13.85$, $b = 13.58$, $c = 9.65$ Å ($a \times b \times c$ basic cell, hereafter) were obtained. On the basis of the actual chemical data for balangeroite, and taking into account both the structure model of Moore (1969) and the empirical formula of Dunn (1979) for gageite, the following unit-cell content was proposed for balangeroite: $(Mg,Fe,Mn,\square)_{42}Si_{15}(O,OH)_{90}$.

As a result of electron-diffraction and transmission-electron microscopy (TEM) studies of balangeroite and gageite, we have revised the interpretation of the crystal structures of these minerals and their polytypic relationships, and we have considered in more general terms the order-disorder phenomena in the whole structural family.

Experimental details

Gageite from Franklin, New Jersey, U.S.A., was kindly provided by Mr. Ewald Gerstmann through the courtesy of P. B. Moore and by the Smithsonian Institution through the courtesy of P. J. Dunn. Oriented thin sections of holotype balangeroite were obtained from R. Compagnoni.

Electron diffraction and imaging were carried out in a Philips 400T electron microscope, as described by, e.g., Mellini et al. (1984). Ground specimens of balangeroite and gageite were studied, but the only ion-thinned specimens were of balangeroite, because of the more limited availability of gageite.

Electron-diffraction data were obtained by selected-area diffraction (SAD) techniques. As balangeroite and gageite develop pronounced {110} cleavage on grinding, controlled tilting experiments were performed with the [001] fiber direction as tilt axis. In this way, the recombination of several [uv0] diffraction patterns displayed an overall view of the whole reciprocal lattice. Views along [001] were also obtained for balangeroite, starting from suitable thin sections.

Pseudocells and true cells

Up to this point, we have introduced two different unit cells, the $a \times b \times c'$ cell of Moore (1969) and the $a \times b \times c$ cell of Compagnoni et al. (1983). Although both cells have been superseded by the results of our electron-diffraction study, we shall frequently refer to the $a \times b \times c$ cell, so closely related to the structural model of Moore (1969), as a useful reference frame. Crystallographic planes and directions in the preceding as well as in the subsequent pages will be referred to that cell, unless otherwise stated.

Figure 1a shows a [100] electron-diffraction pattern taken of balangeroite. Incidentally, such a pattern is almost identical to the [010] pattern, owing to an overall pseudotetragonal symmetry. The sharp, strong spots in that pattern correspond to the $a \times b \times c'$ cell of Moore. A similar distinction between weak reflections with $l = 3n \pm 1$ and strong subcell reflections with $l = 3n$ is evident in Figure 1b, which shows the [1$\bar{1}$0] diffraction pattern. From a series of similar [uv0] diffraction photographs, the whole pattern of balangeroite was obtained (Fig. 2). The corresponding direct lattice may be de-

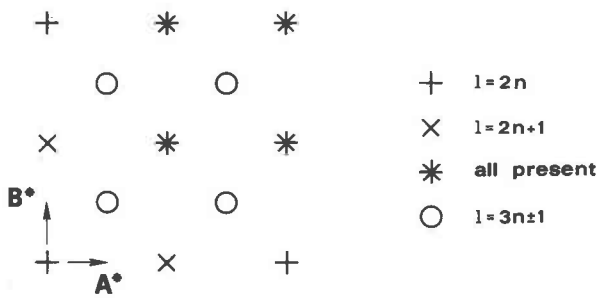

Fig. 2. The diffraction pattern of balangeroite and gageite 2M, with reference to the $2a \times 2b \times c$ cell (i.e., $A \times B \times C$ cell).

scribed in terms of a metrically orthorhombic $2a \times 2b \times c$ C-centered cell, or, otherwise, a primitive cell with unit-cell parameters $a_m = 19.40$, $b_m = 19.40$, $c_m = 9.65$ Å, $\gamma_m = 88.9°$ and related to the basic $a \times b \times c$ cell through the transformation matrix $(1\bar{1}0/110/001)$ (Fig. 3a).

A similar diffraction pattern occurs for gageite, and the corresponding primitive direct cell possesses parameters $a_m = 19.42$, $b_m = 19.42$, $c_m = 9.84$ Å, $\gamma_m = 89.5°$. However, the electron-diffraction study of gageite showed the frequent occurrence of a second electron-diffraction pattern (Fig. 1c) besides that formerly mentioned. The corresponding direct cell has cell parameters $a_t = 14.17$, $b_t = 14.07$, $c_t = 9.84$ Å, $\alpha_t = 76.5°$, $\beta_t = 76.6°$, $\gamma_t = 86.9°$ and is related to the basic $a \times b \times c$ cell through the transformation matrix $(10\frac{1}{3}/01\frac{1}{3}/001)$ (Fig. 3b). It will be shown that the two distinct diffraction patterns correspond to two polytypic modifications of gageite, which, on the basis of the symmetry properties and structural relationships that we are going to discuss, may be conveniently called gageite 2M and gageite 1Tc.

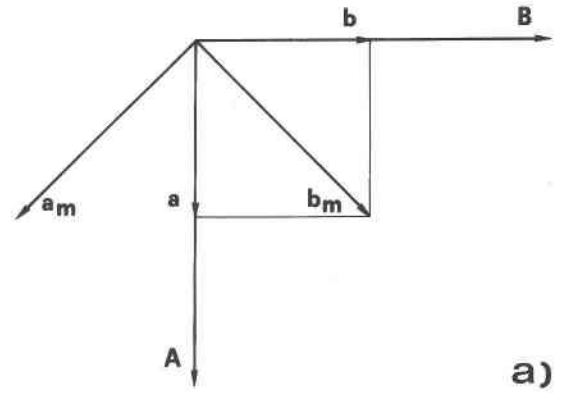

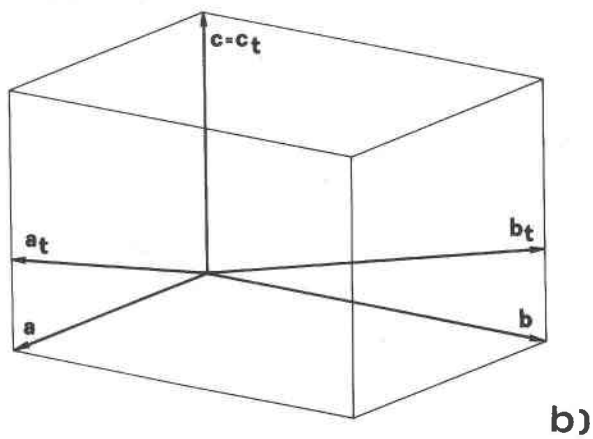

Fig. 3. (a) Geometrical relationships among the $a \times b \times c$ cell, the $2a \times 2b \times c$ C-centered cell and the corresponding $a_m \times b_m \times c_m$ primitive cell for balangeroite and gageite 2M. (b) Geometrical relationships between the triclinic cell of gageite 1Tc and the basic $a \times b \times c$ cell.

The additional module: The four-repeat silicate chain

Any proposed structure model for balangeroite and gageite must take into account (1) the previous structural work of Moore (1969) on gageite; (2) the two different patterns that we observed by electron diffraction; (3) the relationships connecting pseudocells and true cells; (4) the chemical data; (5) the infrared spectrum of balangeroite (Compagnoni et al., 1983), typical of chain silicates in the range 900–1100 cm^{-1}; (6) the fibrous nature of both minerals, with [001] as the fiber axis; and any other physical properties.

As already stated, the structure model of Moore (1969), $R = 0.17$, is plausible as far as the octahedral framework is concerned. However, as stressed by Moore himself and later remarked on by Dunn (1979) and Compagnoni et al. (1983), a more complete and satisfactory model for the distribution of the silicate tetrahedra in the pipelike channels should be proposed. The model must be able to lead naturally from the 3.2-Å c' periodicity, which corresponds to the length of the octahedral edge, to the trebled 9.6-Å c period, without completely destroying the c' translational pseudosymmetry, as required by the very strong intensities of the diffraction spots corresponding to the $a \times b \times c'$ cell.

We assumed that the open [001] channels within the octahedral framework are occupied by a continuous chain of silicate tetrahedra with 9.6-Å periodicity. Such a structural unit corresponds to the four-repeat crankshaft chain of haradaite (Takéuchi and Joswig, 1967). This type of chain is not unusual in mineral structures and, by different degrees of polymerization, gives rise to the double chain of caysichite (Mellini and Merlino, 1978), to the tetrahedral strip of carlosturanite (Mellini et al., 1985), and to a large group of framework silicates, including the feldspars (Smith, 1974). According to our model, the T_4O_{12} chain connects to the octahedral framework through its unshared corners, sandwiching each 3×1 octahedral wall.

Figure 4 shows the interconnection between one tetrahedral chain and the octahedral framework, as seen along the [110] direction, whereas Figure 5 presents the [001] projection, which is common to all the actual and possible structures in this family, showing the distribu-

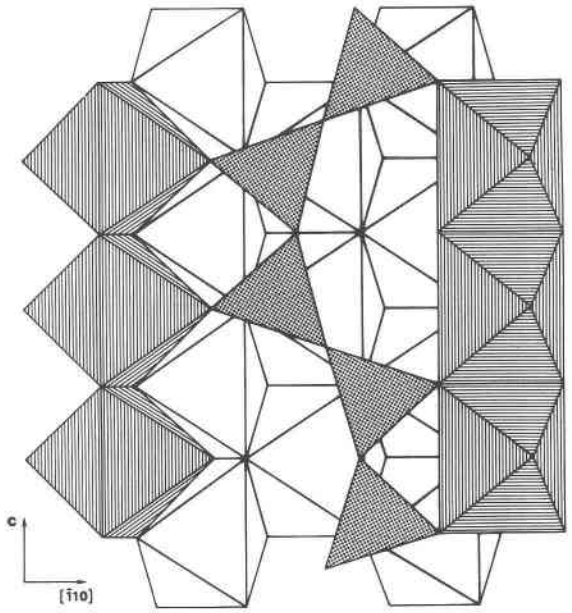

Fig. 4. The connection between tetrahedral chains and octahedral framework, as seen along [110] with respect to the basic $a \times b \times c$ cell.

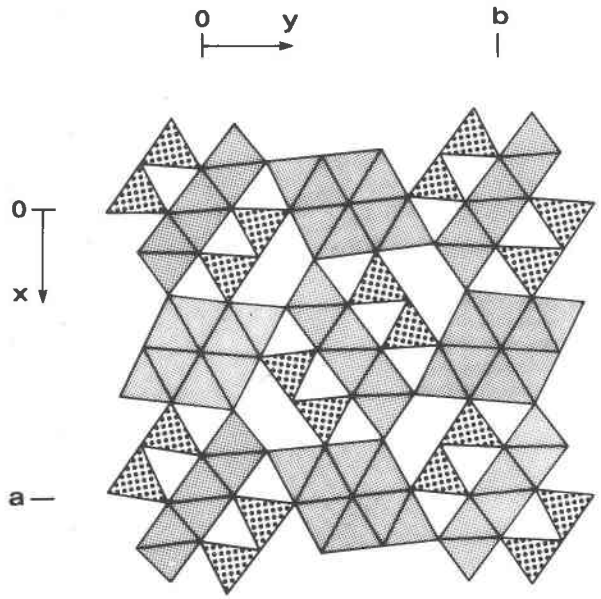

Fig. 5. [001] projection of the crystal structure of balangeroite and gageite, described with reference to the $a \times b \times c$ cell and showing the tetrahedral chains within the channels defined by the 3 × 1 octahedral walls and 2 × 2 octahedral bundles.

tion of the tetrahedral chains in the channels of the octahedral framework. The resulting ideal chemical content of an $a \times b \times c$ unit cell is $M_{42}O_6(OH)_{40}(T_4O_{12})_4$, where M and T indicate octahedral and tetrahedral cations, respectively. The six oxygen atoms not belonging to the tetrahedral chain correspond to anions coordinated to six octahedral cations and located in the central part of the bundles. The hydroxyls correspond to anions coordinated to only three octahedral cations: their number could be lower than 40, because of substitution of oxygen for hydroxyl when the valence of the coordinating cations is higher than 2+.

An isotropic refinement of the gageite structure, based on this model and using the X-ray reflections measured by Moore (1969), improved the R value from 0.17, obtained by Moore, to 0.155 for 612 reflections.

As we found one exceptionally good crystal among those provided by E. Gerstmann, we proceeded to a new intensity-data collection in the $a \times b \times c'$ cell of Moore. A total of 1026 independent reflections were measured on an Ital Structures four-circle automatic diffractometer, with Zr-filtered Mo$K\alpha$ radiation. The atomic coordinates calculated on the basis of our model were refined, together with the isotropic thermal parameters, in the space group *Pnnm*. In a few cycles of least-squares refinement, the R index dropped to 0.049 for 871 reflections with $F_o > 5\sigma(F_o)$.[1]

[1] To obtain a copy of the observed and calculated structure factors, order Document AM-87-333 from the Business Office, Mineralogical Society of America, 1625 I Street, N.W., Suite 414, Washington, D.C. 20006, U.S.A. Please remit $5.00 in advance for the microfiche.

Table 1 reports the positional and thermal parameters for all the atoms, together with the occupancies of Mn and Mg in the M(1) and M(2) octahedral sites. The bond distances in the various polyhedra, calculated on the basis of the coordinates reported in Table 1, appear normal and—as regards those associated with the octahedral framework—in good agreement with those found by Moore (1969). It seems useful to remark that the Mg and Mn contents derived from the structural refinement compare fairly well with those obtained from the chemical data. The parallel refinement of Moore's model, carried out starting with the coordinates given by Moore (1969) and using the same 871 reflections, led to a reliability index of $R = 0.079$.

Revised crystal chemistry

On the basis of the average analyses of balangeroite (Compagnoni et al., 1983) and gageite (Dunn, 1979) and assuming, according to the present structure model, sixteen Si atoms in the $a \times b \times c$ volume, the formulas obtained for balangeroite and for gageite, respectively, are $(Mg_{26.74}Fe^{2+}_{7.99}Fe^{3+}_{3.77}Mn_{1.71}Al_{0.18}Ca_{0.08}Cr_{0.01}Ti_{0.01})_{\Sigma 40.49}Si_{16}O_{55.81}(OH)_{37.35}$ and $(Mg_{11.32}Fe_{0.11}Mn_{28.95}Ca_{0.14}Zn_{2.13})_{\Sigma 42.65}Si_{16}O_{54.53}(OH)_{40.23}$.

The agreement with the ideal cell content is good. The calculated densities are 3.098 and 3.599 g/cm³ for balangeroite and gageite, respectively. These values compare to the observed ones: 2.98 g/cm³ for balangeroite (Compagnoni et al., 1983) and 3.584 (Palache, 1928) and 3.46 g/cm³ (Dunn, 1979) for gageite. New measurements on balangeroite (holotype material, torsion balance) gave values in the range 2.96–3.10 g/cm³ with an average value

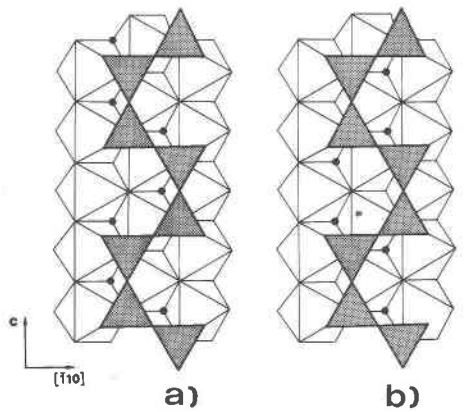

Fig. 6. The two possible TOT modules. Only the upper chain is drawn; filled circles indicate the connection points of the lower chain with the octahedral wall. (a) Upper and lower T chains are shifted by $c/3$. (b) Upper and lower T chains are related by a twofold axis and have common z height.

of 3.06 g/cm³. The agreement is reasonable, taking into account the difficulty in accurately measuring the density of fibrous material, because of the tendency to underestimate density values, as well as, at least for balangeroite, the occurrence of intergrown chrysotile, as discussed in the last part of this paper.

Structural details: Chain shifts and layer sequences

The introduction of the four-repeat tetrahedral chains fairly well explains the chemical data and a number of physical properties, as well as the gross features of the electron-diffraction patterns. The structural results so far obtained are conveniently summarized in Figure 5, which presents the projection of the whole structure along the fiber axis.

It is our present aim to determine the precise and detailed arrangement of the various modules in the two structural forms whose existence we outlined in the previous chapters. In particular we want to derive (1) the way in which the tetrahedral chains attach to both sides of a 3 × 1 octahedral wall—i.e., whether the two chains are placed at the same height, thus building a TOT complex module with a twofold symmetry axis (Fig. 6b), or are displaced by $\pm c/3$ one relatively to the other (Fig. 6a)—and (2) the relationships among the various TOT complex modules that, by interconnection through the octahedral 2 × 2 bundles, build up the two different polytypes.

To these ends we shall consider, beyond the simple geometrical features that we have so far discussed, more subtle features in the diffraction patterns, namely, the systematic absences that appear in the patterns and the intensity distribution among the various classes of reflections. We shall pay attention mainly to the monoclinic

Table 1. Gageite substructure

	x	y	z	B	M
M(1) = 0.36 Mn + 0.64 Mg	0	0	½	0.66(5)	2.00
M(2) = 0.46 Mn + 0.54 Mg	0.3376(1)	0.3840(1)	½	0.76(4)	4.00
M(3) = 1.00 Mn	0.4225(1)	0.1518(1)	0	0.99(3)	4.00
M(4) = 1.00 Mn	0.1016(1)	0.4991(1)	0	0.82(3)	4.00
Si(1)	0.2109(2)	0.0967(2)	0.4568(15)	0.47(6)	2.67
Si(2)	0.0671(2)	0.1948(2)	0.0355(18)	0.54(6)	2.67
O(1)	½	0	0	1.02(10)	2.00
O(2)	0.3313(4)	0.0915(4)	½	1.11(8)	4.00
O(3)	0.3420(3)	0.2845(4)	½	1.05(8)	4.00
O(4)	0.4918(3)	0.3988(3)	½	1.07(7)	4.00
O(5)	0.3489(4)	0.4917(4)	½	1.22(8)	4.00
O(6)	0.1878(3)	0.3904(3)	½	0.84(7)	4.00
O(7)	0.0201(4)	0.3056(4)	½	1.17(7)	4.00
O(8)	0.1922(10)	0.1425(10)	0	0.98(20)	1.33
O(9)	0.1640(6)	0.1823(6)	0.7479(29)	0.53(13)	2.67
O(10)	0.1136(11)	0.1919(10)	½	0.73(20)	1.33

Bond distances (in Å)

M(1)–O(4) (×4)	2.151	M(3)–O(2) (×2)	2.227
–O(5) (×2)	2.089	–O(7) (×2)	2.201
M(2)–O(3) (×2)	2.130	–O(1)	2.336
–O(5) (×2)	2.209	–O(3)	2.130
–O(4)	2.132	M(4)–O(1) (×2)	2.267
–O(6)	2.068	–O(6) (×2)	2.179
Si(1)–O(2)	1.664	–O(2)	2.155
–O(5)	1.663	–O(7)	2.270
–O(8)	1.664	Si(2)–O(4)	1.649
–O(9)	1.637	–O(7)	1.643
		–O(9)	1.628
		–O(10)	1.683

Note: Atomic coordinates, isotropic temperature factors (in Å²) and multipliers, with, in parentheses, the standard deviations.

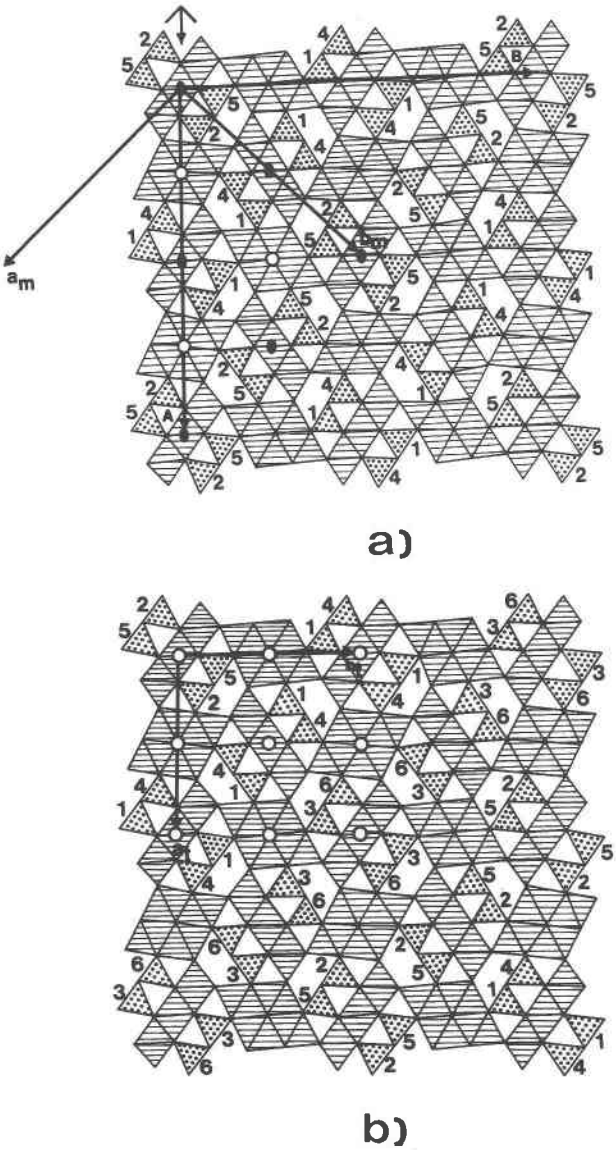

Fig. 7. Crystal structure drawings of both polytypes. The digits give the height, in $C/6$ units, of the different tetrahedral chains with reference to the bridging oxygen atoms. The symmetry elements are indicated. (a) Balangeroite and gageite 2M; both the double $A \times B \times C$ cell and primitive $a_m \times b_m \times c_m$ cell are indicated. (b) Gageite 1Tc; the primitive triclinic cell is indicated.

form, and the analysis will be carried out on its diffraction pattern, with reference to the C-centered cell characterized by translation periods $A = 2a$, $B = 2b$, $C = c$ ($2a \times 2b \times c$ cell).

Inspection of the systematic absences in the diffraction pattern of Figure 2 shows, besides the absences due to C-centering, additional systematic absences for $k = 2n + 1$ and $l = 3n$. These are obviously not space-group extinctions and must result from a particular structural arrangement. An arrangement that naturally leads to the C-centering and to systematic absences of the kind observed

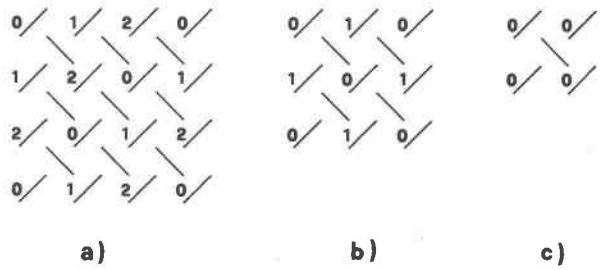

Fig. 8. Schematic drawings of the different polytypes, with indications, in $C/3$ units, of the relative heights of the TOT modules. (a) Triclinic form. (b) Monoclinic form. (c) Hypothetical orthorhombic form.

consists of (110) structural layers that follow each other according to the alternating stacking vectors $\mathbf{t}_1 = \mathbf{B}/2 + \mathbf{C}/3$ and $\mathbf{t}_2 = \mathbf{B}/2 - \mathbf{C}/3$. According to this model, the general structure factor F_{hkl} is given by the expression

$$F_{hkl} = \{\Sigma_j f_j \exp[2\pi i(hx_j + ky_j + lz_j)]\} \cdot \{1 + \exp[2\pi i(k/2 + l/3)]\}, \quad (1)$$

where x_j, y_j, and z_j are the coordinates of the atoms in the layer, with reference to the A, B, and C cell parameters.

Within the kinematical approximation, the second power of the last factor will modulate the overall intensity distribution, depending on the value of $k/2 + l/3$. In particular, the second power of the last factor vanishes when $k = 2n + 1$ and $l = 3n$, leading to the systematic absences actually observed. More generally, it may assume four distinct values:

0 for $3k + 2l = 6n + 3$
1 for $3k + 2l = 6n \pm 2$
3 for $3k + 2l = 6n \pm 1$
4 for $3k + 2l = 6n$.

Although the observed intensity depends also on the first factor—the Fourier transform of the layer—in expression 1, as well as on dynamical effects, the second factor will largely imprint the overall intensity distribution. It is satisfying to find that the reflections are neatly distributed in four classes according to their intensity, as follows:

		I_{obs}	I_{calc}
$k = 2n + 1$	$l = 3n$	absent	0
	$l = 3n \pm 1$	medium–strong, diffuse	3
$k = 2n$	$l = 3n$	very strong, sharp	4
	$l = 3n \pm 1$	weak, diffuse	1

where the terms in the I_{calc} column recall the values assumed by the second power of the modulating term in the expression of the structure factor. Figure 1b is, in this respect, particularly convincing, as it displays simultaneously the four classes of intensities.

A second highly compelling check of the validity of the model lies in the fact that it naturally leads to a sound structural scheme for the triclinic form. In fact by sub-

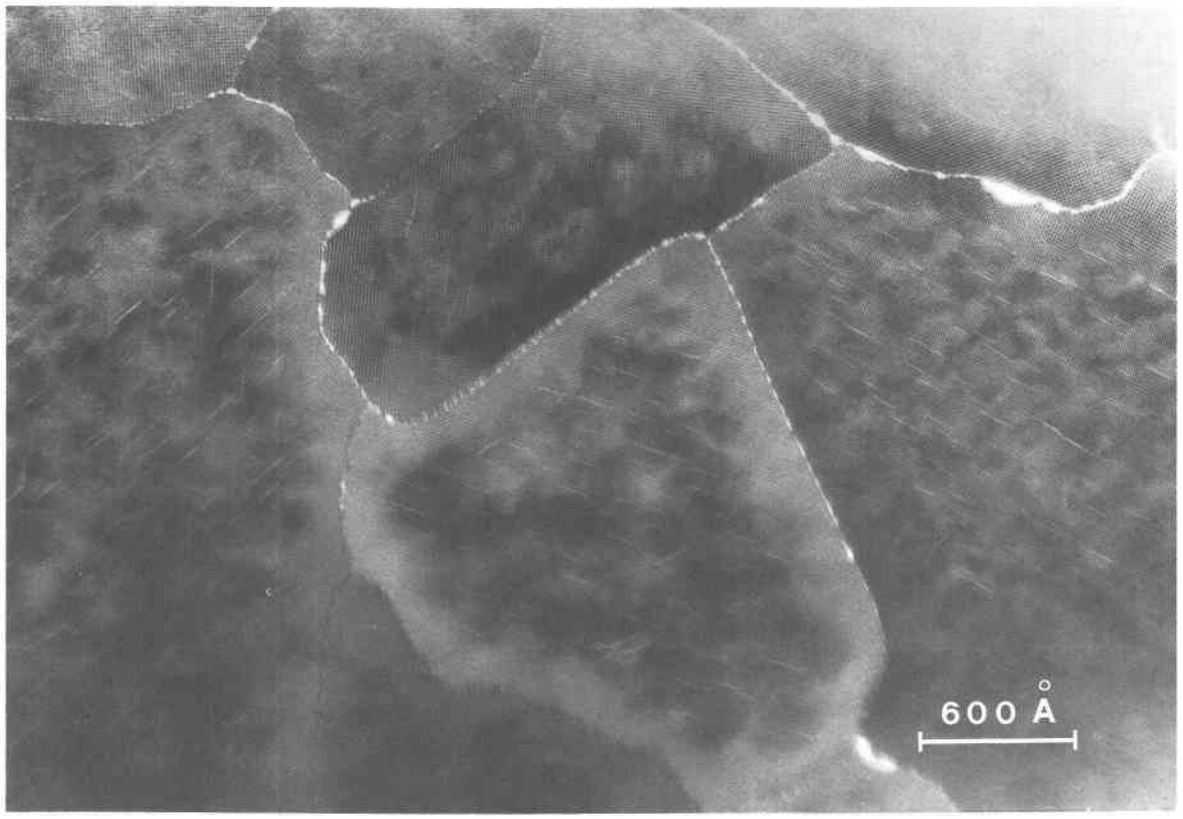

Fig. 9. Fiber texture of balangeroite, as seen along the [001] fiber axis. The white contrast lines in each fibril develop within the (100) plane.

stituting the vector sequence $\mathbf{t}_1\mathbf{t}_2\mathbf{t}_1\mathbf{t}_2 \ldots$, realized in the monoclinic phase, with the sequence $\mathbf{t}_1\mathbf{t}_1\mathbf{t}_1\mathbf{t}_1 \ldots$ (or $\mathbf{t}_2\mathbf{t}_2\mathbf{t}_2\mathbf{t}_2 \ldots$), we obtain a structure with lattice parameters corresponding to those observed for the triclinic form.

With regard to the internal structure of the slab, it is necessary to consider the relative arrangement of the complex modules in the slab and the relative heights of the tetrahedral chains that sandwich the 3 × 1 walls. These features can be deduced by taking advantage of the non–space-group systematic absences that were observed, in the $0kl$ plane, for $k + 2l = 4n + 2$ and, in the $h0l$ plane, for $h + 2l = 4n + 2$ (Figs. 1a, 2). These absences were observed in the diffraction pattern of Figure 2 and are interpreted as being dependent on the internal arrangement of the basic structural layer.

The absences for $h + 2l = 4n + 2$ may be easily explained if we assume that in the basic layer, adjacent TOT complex modules are related through a pseudoglide normal to B and with translational component $A/4 + C/2$: the operation is described as a pseudoglide because of its partial character, as it does not refer to the whole crystal. Furthermore, the observed absences for $k + 2l = 4n + 2$ imply that the two modules are related also by a similar pseudoglide normal to A. The presence of both pseudoglides demands a twofold axis along [001] in each TOT module, which indicates that Figure 6b represents the correct scheme for the assemblage of tetrahedral chains and octahedral walls.

Figure 7a summarizes the results of the preceding discussion by giving the representation of the structural topology of balangeroite and gageite 2M. The level of the tetrahedral chains is denoted by the height, in $C/6$ units, of the bridging oxygen atoms in both disilicate groups placed along [001] that build up the repeat unit of the chain. In the same figure we have outlined both unit cells, the C-centered double cell, with A and B translations, and the simple cell with a_m and b_m translation parameters. The symmetry elements are also shown in the latter cell: twofold axes, inversion centers at levels 0 and 3, in $c_m/6$ units, and n glides at levels 1.5 and 4.5, in $c_m/6$ units. The resulting space-group symmetry is $P2/n$, with the twofold axis in the **c** direction; it seems useful to remark that a nonstandard origin has been chosen on the twofold axis to maintain a closer relationship with Moore's cell and the basic $a \times b \times c$ cell.

Similarly, Figure 7b gives the structural arrangement in gageite 1Tc. The heights of the various tetrahedral chains are indicated, and we have outlined the unit-cell translations a_t and b_t, both starting from the inversion center at level 2, in $c_t/6$ units, assumed as origin, and ending on inversion centers at level 4. The resulting space group is $P\bar{1}$.

Figure 8 presents schematic drawings where the composite TOT modules are represented by segments oriented as the projection of the octahedral walls, with the relative heights of the modules indicated. The structural schemes for both monoclinic and triclinic forms are compared with the hypothetical $a \times b \times c$ structure, which is orthorhombic and has space-group symmetry *Pnnm*. Note that no electron-diffraction evidence was found for the existence of individual domains with such a simple arrangement, characterized by the absence of shifts in the relative height of the TOT modules.

Balangeroite and gageite as OD structures

The polytypic relationship between the monoclinic and triclinic modifications may be conveniently treated in more formal terms according to the theory of OD structures (Dornberger-Schiff, 1956, 1964, 1966), which consist of equivalent layers. The monoclinic structural type in balangeroite and gageite 2M and the triclinic type in gageite 1Tc correspond to distinct ordered members of a whole OD-structure family that, according to the theory, includes those structures in which all the pairs of adjacent layers are geometrically equivalent. Each structure, in the present family, may be described as consisting of equivalent layers, with symmetry $2/m$ and translation periods $a_m = 19.42$, $c_m = 9.84$ Å (we report here the metrical values obtained for gageite). The "width" of the layer is $b_o = b_m/2 = 9.7$ Å, and $\gamma_m = 89.5°$. Adjacent layers are related by a vector $\mathbf{t}_1 = -\mathbf{a}_m/2 + \mathbf{b}_o + \mathbf{c}_m/3$ or $\mathbf{t}_2 = -\mathbf{a}_m/2 + \mathbf{b}_o - \mathbf{c}_m/3$.

The pairs of layers obtained in either case are geometrically equivalent. Therefore any sequence of $\mathbf{t}_1$ and $\mathbf{t}_2$ vectors defines a member of the family, and infinite ordered polytypes, as well as disordered forms, are thus possible in the family. However, only two members exist with the maximum degree of order, the so-called MDO structures according to OD-structure theory. These are the members in which all triples, quadruples . . . , and n-tuples of consecutive layers are geometrically equivalent. They correspond to the vector sequences $\mathbf{t}_1\mathbf{t}_1\mathbf{t}_1\mathbf{t}_1 \ldots$ (or $\mathbf{t}_2\mathbf{t}_2\mathbf{t}_2\mathbf{t}_2 \ldots$) and $\mathbf{t}_1\mathbf{t}_2\mathbf{t}_1\mathbf{t}_2 \ldots$. As already discussed, the first sequence is realized in gageite 1Tc with only one layer in the triclinic unit cell; the second is realized in gageite 2M and, with a different chemistry, in balangeroite. Both gageite 2M and balangeroite contain two layers in the monoclinic primitive cell.

The symmetry characteristics of the OD-groupoid family, which plays a role analogous to that of the space group for a single ordered crystal, is given by the collection of all the transformations of space that bring a layer into coincidence with itself, λ-PO operations (PO = partial operation), or with the next layer, σ-POs. The description and derivation of the OD-groupoid families were discussed by Dornberger-Schiff and Grell-Niemann (1961) and Dornberger-Schiff and Fichtner (1972). In the present case the OD-groupoid family is

$$\begin{matrix} P\,1 & (1) & 2/m \\ \{1 & (1) & 2_{2/3}/n_{1,2}\} \end{matrix}$$

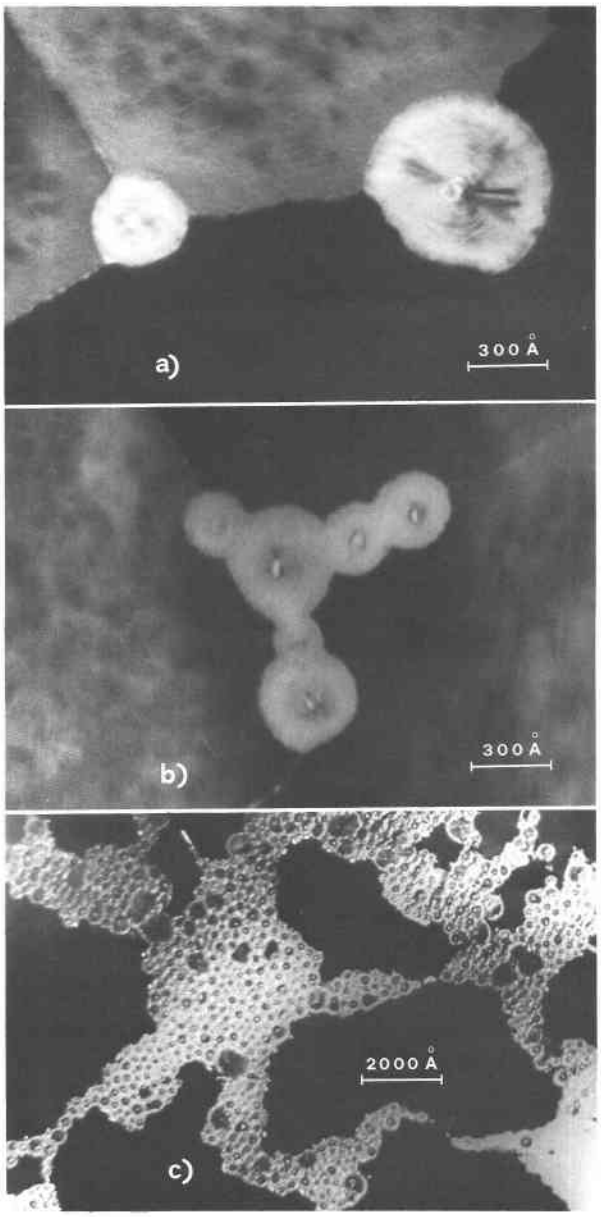

Fig. 10. Chrysotile substituting for balangeroite. (a) Individual chrysotile fibers neucleate at triple junctions. (b) Growth of chrysotile develops along the interfaces between two adjacent balangeroite fibers. (c) Advanced substitution of chrysotile fibrils for balangeroite.

where, as usual, the first line of the symbol gives the λ-POs, namely, the plane space group of the single layer; the second line gives the set of σ-POs. The brackets around the second position of each line indicate that only the basic vectors $\mathbf{a}_m$ and $\mathbf{c}_m$ are translation vectors that correspond to the translations of the structural layer; the third vector $\mathbf{b}_o$ is not a translation vector.

According to the symbolism, two successive layers are related through a twofold screw axis with translational component 2/6 c_m and also through a glide normal to $\mathbf{c}_m$

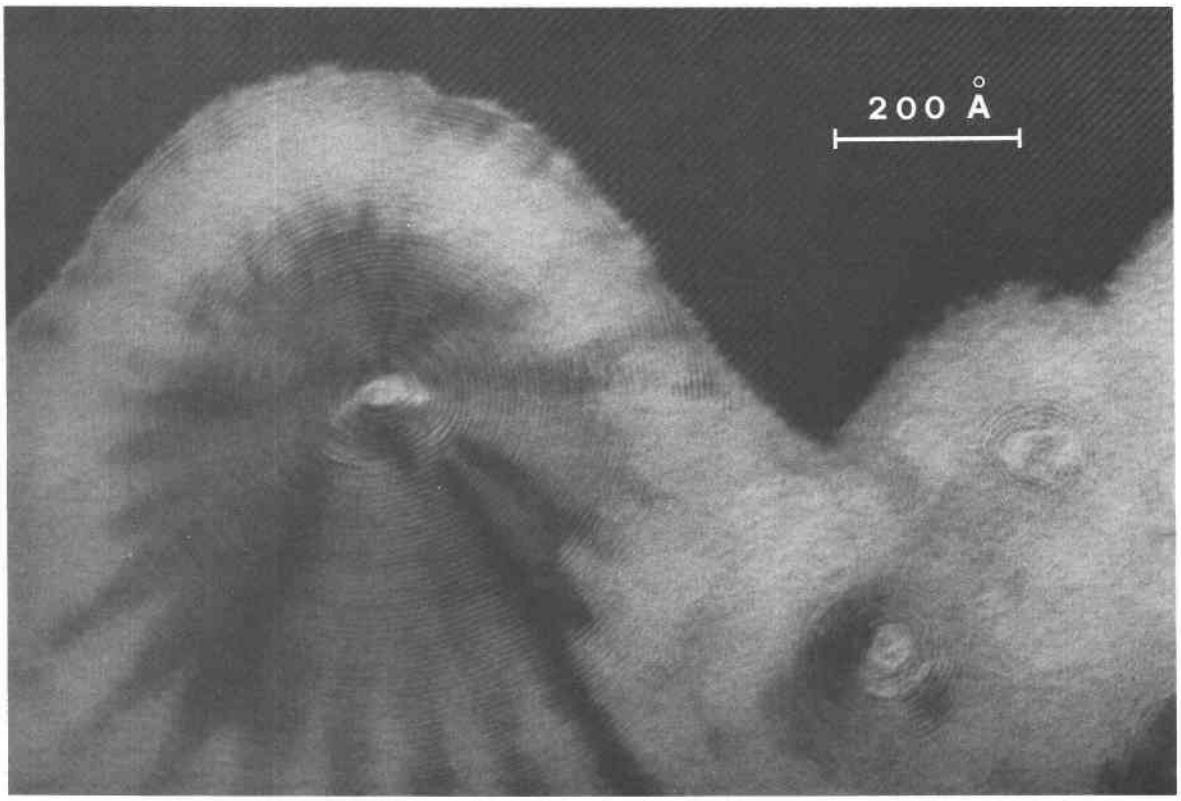

Fig. 11. Contact between the curled chrysotile layers and the balangeroite fibers.

with translational components $-a_m/2 + b_o$. A pair of layers related through the screw operation $2_{2/3}$ indicated in the symbol is geometrically equivalent to a pair of layers related through a screw $2_{2/3}$, where the translational component is in the opposite direction. If $2_{2/3}$ operation is followed by a $2_{2/3}$ operation, the first and third layer are at the same level, and the twofold axis of the single layer is now valid for the whole structure; moreover, the σ-PO $n_{1,2}$ is continued, becoming a true n glide of the whole structure. The overall space-group symmetry of the resulting structure is therefore $P112/n$. On the other hand, if $2_{2/3}$ is followed by $2_{2/3}$, the first and third layers are at different levels (2/3 c_m apart), and the twofold axes are no longer total symmetry elements; moreover the $n_{1,2}$ glide is not continued from the second to the third layer, but transposed by 1/3 c_m. Only inversion centers now act as total symmetry elements, and the overall space group symmetry is therefore $P\bar{1}$.

Besides these two ordered polytypes, the MDO members in the family, a potentially infinite series of ordered structures may be conceived, corresponding to periodic sequences of $2_{2/3}$ and $2_{2/3}$ operations. Aperiodic sequences of these σ-POs will lead to disordered members of the family.

The different patterns corresponding to the different structures of the family present identical reflections of the type $l = 3n$. These "family reflections" are always sharp and correspond to the "superposition structure," just that substructure described in Moore's work (1969). For $l \neq 3n$, the different members of the family present different patterns, with diffuse streaks parallel to $\mathbf{b}_m^*$ in the disordered members and sharp spots for the ordered ones. The various diffraction patterns we studied were indicative of various degrees of structural order, from those with nearly continuous streaks without maxima at all, to those presenting nearly sharp maxima in the reciprocal lattice positions corresponding to the monoclinic and triclinic polytypes. These two extreme cases correspond, respectively, to disordered sequences of $\mathbf{t}_1$ and $\mathbf{t}_2$ stacking vectors (aperiodic sequences of $2_{2/3}$ and $2_{2/3}$) and to large domains of either polytypes. In intermediate cases, the wider the maxima the smaller the volume of the ordered domains and the larger the disordered portion of the crystal.

Texture and fault contrast in balangeroite

The lattice images obtained along the fiber axis (Fig. 9) show that the balangeroite bundles consist of randomly rotated single fibers with cross sections in the range 500–5000 Å. The outer shape of the fibers is somewhat irregular and largely determined by the interlocking fibers. However, surfaces with simple indices, such as {100}, {010}, {110}, {1$\bar{1}$0}, with reference to the $2a \times 2b \times c$ unit cell, are the most common. These faces correspond to the most populated octahedral planes in the structures.

Figure 9 shows also the occurrence of widespread fault-

ing. Either within (100) or, less frequently, (110) planes, white lines of contrast are present throughout the fibers. Apparently, these faulted regions separate parts where similar contrast patterns are present. The fault density decreases with decreasing crystal thickness, perhaps suggesting that the faults responsible for this contrast are not infinitely extended along the observation axis and that the greater the thickness of the crystal, the higher the probability of seeing the fault contrast. Regarding the structural nature of the faults, no conclusive proof can be given. Most probably the fault contrast arises from features other than faulted polytypic sequences, since contrast develops on the (100) rather than on the (110) plane; moreover, indications exist that the fault does not affect the whole crystal thickness, as would be required by a polytypic fault. Also, stacking faults parallel to the observation direction would not produce any important contrast, when using the [001] bright-field conditions we adopted for HR imaging. A possible explanation is the occurrence of Wadsley defects, with the insertion of structural modules other than the 3×1 octahedral wall and 2×2 octahedral bundles. One example might be 3×2 modules within the overall regular tesselation, with concerted vacant tetrahedral sites.

Metamorphic reactions involving balangeroite

In several ways the fiber texture in balangeroite recalls that found in another 9-Å asbestiform silicate, carlosturanite (Compagnoni et al., 1985; Mellini et al., 1985). In particular, balangeroite is also intergrown with parallel chrysotile fibers. The relative abundance of the two minerals is widely variable (Fig. 10). Figure 11 shows in more detail the contact between balangeroite and chrysotile, with the latter encroaching into balangeroite. The whole sequence of images can be explained by assuming that chrysotile was replacing balangeroite. In the earliest stage of replacement (Fig. 10a), chrysotile would develop just at the junction of three balangeroite fibers, where structural misfit is maximum and fluid circulation is most favored. The chrysotile growth would continue along the boundaries between two balangeroite fibers (Fig. 10b), and clusters of chrysotile fibers would be formed around the first growth centers (Fig. 10c), but the original balangeroite texture would be still identifiable. Finally, extensive replacement of chrysotile for balangeroite would obscure the original textural relationships within balangeroite (Mellini, 1986).

The TEM observations closely parallel those made by Compagnoni et al. (1983) using optical microscopy. They observed balangeroite that developed quite early in the Balangero serpentinite and also balangeroite pseudomorphs after orthopyroxene in specimens from the Lanzo massif. Chrysotile was formed later, as deduced from the TEM images, and was successively corroded by metamorphic olivine, before finally being transformed into antigorite. Therefore, balangeroite turns out to be an intermediate mineral within the retrograde metamorphism of the Balangero ultramafic body. In particular it would be formed from orthopyroxenes through the reaction $21Mg_2Si_2O_6 + 20H_2O = Mg_{42}O_6(OH)_{40}(Si_4O_{12})_4 + 26SiO_2$ and would transform to chrysotile through the reaction $Mg_{42}O_6(OH)_{40}(Si_4O_{12})_4 + 12SiO_2 + 8H_2O = 14Mg_3Si_2O_5(OH)_4$.

Acknowledgments

We are grateful to P. J. Dunn (Smithsonian Institution) for kindly providing specimens of gageite from Franklin (R6639, C6803); P. B. Moore (Chicago) who sent us the set of reflection intensities collected in 1969 and some beautiful crystals of gageite from Franklin, selected from the specimen no. 1140 in the collection of Ewald Gerstmann, to whom we extend our acknowledgments; R. Compagnoni (Torino) who provided us with oriented thin sections of holotype balangeroite; M. Pasero (Pisa) who collected the new set of intensity data and carried out the least-squares refinement.

This research has been supported by M.P.I. 40% grants.

References

Compagnoni, R., Ferraris, G., and Fiora, L. (1983) Balangeroite, a new fibrous silicate related to gageite from Balangero, Italy. American Mineralogist, 68, 214–219.

Compagnoni, R., Ferraris, G., and Mellini, M. (1985) Carlosturanite, a new asbestiform rock-forming silicate from Val Varaita, Italy. American Mineralogist, 70, 767–772.

Dornberger-Schiff, K. (1956) On order-disorder structures (OD-structures). Acta Crystallographica, 9, 593–601.

——— (1964) Grundzuge einer Theorie der OD-Strukturen aus Schichten. Abhandlungen der Deutschen Akademie der Wissenschaften, Berlin.

——— (1966) Lehrgang uber OD-Strukturen. Akademie Verlag, Berlin.

Dornberger-Schiff, K., and Fichtner, K. (1972) On the symmetry of OD-structures consisting of equivalent layers. Kristall und Technik, 7, 1035–1056.

Dornberger-Schiff, K., and Grell-Niemann, H. (1961) On the theory of order-disorder (OD) structures. Acta Crystallographica, 14, 167–177.

Dunn, P.J. (1979) The chemical composition of gageite: An empirical formula. American Mineralogist, 64, 1056–1058.

Gjonnes, J., and Moodie, A.F. (1965) Extinction conditions in the dynamic theory of electron diffraction. Acta Crystallographica, 19, 65–67.

Mellini, M. (1986) Chrysotile and polygonal serpentine from Balangero serpentinite. Mineralogical Magazine, 50, 301–306.

Mellini, M., and Merlino, S. (1978) Caysichite: A double crankshaft chain structure. Canadian Mineralogist, 16, 81–88.

Mellini, M., Merlino, S., and Pasero, M. (1984) X-ray and HRTEM study of sursassite: Crystal structure, stacking disorder, and sursassite-pumpellyite intergrowth. Physics and Chemistry of Minerals, 10, 99–105.

Mellini, M., Ferraris, G., and Compagnoni, R. (1985) Carlosturanite: HRTEM evidence of a polysomatic series including serpentine. American Mineralogist, 70, 773–781.

Moore, P.B. (1969) A novel octahedral framework: Gageite. American Mineralogist, 54, 1005–1017.

Palache, C. (1928) Mineralogical notes on Franklin and Sterling Hill, New Jersey. American Mineralogist, 13, 297–329.

Smith, J.V. (1974) Feldspar minerals. Springer, Heidelberg.

Takéuchi, Y., and Joswig, W. (1967) The structure of haradaite and a note on the Si–O bond lengths in silicates. Mineralogical Journal, 5, 98–123.

Manuscript received May 22, 1986
Manuscript accepted November 20, 1986